Research paper

Calcined Mg/Al layered double hydroxides as efficient adsorbents for polyhydroxy fullerenes

Yanping Zhu[a,b], Runliang Zhu[a,*], Qingze Chen[a,b], Minwang Laipan[a,b], Jianxi Zhu[a], Yunfei Xi[c,d], Hongping He[a]

[a] CAS Key Laboratory of Mineralogy and Metallogeny/Guangdong Provincial Key Laboratory of Mineral Physics and Materials Research & Development, Guangzhou Institute of Geochemistry, Chinese Academy of Sciences (CAS), Guangzhou 510640, China
[b] University of Chinese Academy of Sciences, Beijing 100049, China
[c] School of Chemistry, Physics and Mechanical Engineering, Queensland University of Technology (QUT), GPO Box 2434, Brisbane, Queensland 4001, Australia
[d] Institute of Future Environments, Queensland University of Technology (QUT), GPO Box 2434, Brisbane, Queensland 4001, Australia

ARTICLE INFO

ABSTRACT

The environmental behaviors and pollution control of engineered nanomaterials are drawing increasing interests nowadays. This work showed that the calcined layered double hydroxides (LDH), i.e., layered double oxides (LDO), could effectively adsorb polyhydroxy fullerenes (PHF) from aqueous solution. The maximum adsorption capacity of LDO reached ~476 mg/g, much higher than that on LDH (~47 mg/g) and activated carbon (~28 mg/g). All of the three equilibrium adsorption isotherms could be well fitted with the Langmuir equation. The high adsorption capacity of PHF on LDO can be attributed to the enhanced accessibility to the adsorption sites for PHF during structural reconstruction of LDO. In addition, the rehydrated LDH, with a net positive surface charge, has high affinity for negatively charged PHF through an electrostatic interaction. Cl^-, CO_3^{2-}, and SO_4^{2-} could slightly enhance the adsorption of the PHF on LDO, while HPO_4^{2-} showed an evident inhibiting effect in the whole concentration range of PHF. The adsorbents before and after the adsorption of PHF were characterized by XRD, FT-IR, and TG. The obtained results indicated that the adsorbed PHF could not intercalate into the interlayer spaces of the reconstructed LDH, but could effectively compete with CO_3^{2-} during the adsorption process.

1. Introduction

Carbon-based nanomaterials such as fullerenes, carbon nanotubes, graphene, and graphitic carbon nitride have received increasing interest nowadays because of their unique physicochemical properties and potential applications in a wide range of fields (Jordá-Beneyto et al., 2007; Mauter and Elimelech, 2008; Dai et al., 2012; Jiang et al., 2012; Cha et al., 2013). As most of the engineered carbon nanomaterials will eventually end up in the environment (Nowack and Bucheli, 2007), their potential adverse effects on human health and environment require serious attentions. In this case, their environmental behaviors and toxicity to organisms have been investigated by a number of studies (Sayes et al., 2004; Jia et al., 2005; Perez et al., 2009; Turco et al., 2011; Song et al., 2012; Fortner et al., 2012; Zhu et al., 2013).

Among the various carbon nanomaterials, fullerenes and their derivatives as a family of carbon nanomaterials have potential applications in a wide range of areas, e.g., as biomedicine (Djordjevic and Bogdanovic, 2008; Markovic and Trajkovic, 2008), catalyst (Niu et al., 2011), adsorbents for contaminants (Cheng et al., 2004), hydrogen storage (Yoon et al., 2007), nanofillers for nano-composites (Jung et al., 2010), and antioxidant in cosmetics (Gharbi et al., 2005), etc. As such, the research enthusiasm on this family of carbon nanomaterials is ever increasing, leading to a 'fullerene fever'. As the polyhydroxy fullerenes (i.e., PHF) have high solubility in bulk water while retaining most of the physicochemical properties of fullerenes, it can be conveniently applied in aqueous environment (Djordjevic and Bogdanovic, 2008; Niu et al., 2011; Georgieva et al., 2013). In addition, PHF have been identified as the main products during the exposure of fullerenes to the environment. Many factors such as UV light irradiation, interaction with oxidants (such as hydroxyl radicals) (Lee et al., 2010; Qu et al., 2010; Wu et al., 2014), and interaction with microbes (Chae et al., 2014), can transform fullerenes into PHF.

However, many researchers found that PHF presented cytotoxicity to both bacteria and human cell (Sayes et al., 2004; Isakovic et al.,

2006; Yamawaki and Iwai, 2006). For example, Isakovic et al. (2006) found that PHF could cause cell membrane damage, lipid peroxidation, and necrotic cell death due to a direct generating of reactive oxygen species. Yamawaki and Iwai (2006) found that PHF represented potential risk for cardiovascular diseases, including atherosclerosis and ischemic heart disease. As such, much attention should be paid to the pollution control of PHF in aqueous solution. As both fullerenes and PHF are relatively resistant to biodegradation and chemical attack because of their sp2 hybridized carbon-carbon bonds and toxicity for bacteria (Heyman, 1991; Perez et al., 2009; Avanasi et al., 2014), therefore, adsorption may be a relatively suitable approach for the removal of PHF from aqueous solution, in which choosing proper adsorbents is of critical importance.

With nano-sized layered structure, some clays, such as layered double hydroxides (LDH) and montmorillonite, generally have large surface area, charged layers, and exchangeable ions between the layers (Cavani et al., 1991; He et al., 2010; Zhu et al., 2016). As such, they can effectively adsorb some ions from water through an ion-exchange process (Fortner et al., 2012; Chen et al., 2016). Chen et al. (2016) found that cationic polyethylenimine-modified montmorillonite had high efficiency for the removal of PHF from aqueous solution. Given that PHF are generally negatively charged (Georgieva et al., 2013), LDH, also known as anionic clays, may be good adsorbents for PHF. LDH consist of brucite-like hydroxide sheets, where partial substitution of trivalent for divalent cations results in a positive sheet charge compensated by anions within interlayer spaces (Cavani et al., 1991). One of the interesting characteristics of LDH is that their calcined products, also known as LDO, can rehydrate and recover to LDH in aqueous environment. Previous studies showed that LDO may be more effective adsorbents than LDH in the adsorption of anions from water, as the adsorption of contaminants simultaneously happens with the rehydrating of LDH. In this case, the interlayer spaces (i.e., the adsorption sites) of the rehydrated LDH can be better accessed by contaminants (Zhu et al., 2005; Lv et al., 2008; Crepaldi et al., 2002).

This work examined the adsorption capacity of PHF on LDH and LDO. As activated carbon has been widely used as adsorbent for various contaminants because of its high specific surface area, high adsorption capacity, and low-selectivity for pollutants (Faria et al., 2004; Nakagawa et al., 2004), the adsorption of PHF on a commercial activated carbon was compared as well. In addition, the structures of LDO after PHF adsorption were characterized by XRD, FT-IR, and TG.

2. Experimental

2.1. Materials

PHF were obtained from Suzhou Dade Carbon Nanotechnology Co., Ltd. Activated carbon was purchased from Taishan City Guangdong Overseas Reagent Plastic Co., Ltd. All reagents were used as received. All labware were washed by ultra-pure water (> 18 MΩ/cm) before the experiments.

2.2. Preparation of LDH and LDO

A co-precipitation method following Reichle (Reichle, 1986) with some modifications was used to prepare $Mg/Al\text{-}CO_3\text{-}LDH$. Briefly, 3.5 mol NaOH and 0.943 mol Na_2CO_3 were dissolved in 1000 mL deionized water to which 700 mL mixed solution containing 0.5 mol $Al(NO_3)_3 \cdot 9H_2O$ and 1.0 mol $Mg(NO_3)_2 \cdot 6H_2O$ (Mg: Al molar ratio = 2:1) was added at a rate of 1.0 mL/min under vigorous stirring. The resulting slurry was aged at 80 °C for 24 h while stirring. After cooling to room temperature, the slurry was centrifuged and washed using deionized water at least eight times to remove free ions. Then the material was dried at 80 °C over night, ground and passed through a 100-mesh sieve. Part of the resulting material was calcined at 500 °C for 3 h to obtain LDO. The LDH sample and LDO sample were then placed in a CaO desiccator.

2.3. Adsorption experiments

The adsorption kinetics of the contaminants were conducted with the reaction time in the range of 5 min to 48 h to determine the equilibration time. In particular, 0.02 g LDO, LDH, or activated carbon were dispersed in 0.02 L of PHF solutions with the concentrations at 250, 25, and 25 mg/L, respectively. Different concentrations of PHF were used because these adsorbents have different adsorption capacity. The mixture was stirred at 200 rpm and 25 °C in a shaking table. After adsorption, the suspensions were centrifuged at 4200 rpm for 15 min.

Equilibrium adsorption experiments were carried out to determine the adsorption capacity of PHF on LDO, LDH, and activated carbon. Equilibrium studies were conducted in 0.05 L Teflon tubes by mixing 0.02 L of PHF solution with 0.02 g LDO, LDH, or activated carbon. The mixture was stirred at 200 rpm and 25 °C in a shaking table for 12, 12, and 24 h (equilibration time was selected according to the adsorption kinetic curve results), respectively. The suspensions were centrifuged at 4200 rpm for 15 min.

Cl^-, SO_4^{2-}, or $H_2PO_4^-$ was selected to study the effect of co-existing anions on PHF adsorption by LDO. The experiment was conducted in the solution containing 800 mg/L (~7 mM) PHF, at which the adsorption amount of PHF on LDO has almost reached maximum. Specifically, 0.02 g LDO was dispersed in 0.02 L of solution containing both PHF and a co-existing anion (Cl^-, SO_4^{2-}, or $H_2PO_4^-$), with the concentration of ~7 mM for PHF and 0.14 M for the co-existing anion, respectively. After shaking of the adsorbent mixtures at 25 °C for 12 h, the supernatants were separated by centrifugation at 4200 rpm for 15 min.

The concentration of PHF was measured spectrophotometrically by monitoring the absorbance at 230 nm (maximum absorption wavelength was confirmed by the full wave scanning) using a UV–Vis (759S, Shanghai JingHua Instrument Co. Ltd., China) (Krishna et al., 2006). The full wave scanning also showed that Cl^-, SO_4^{2-}, and $H_2PO_4^-$ had no noticeable absorption at 230 nm. All batch experiments were carried out in triplicate and the error bars were displayed in the figures.

2.4. Characterization

In order to investigate the adsorption mechanism of PHF on LDO and the structure of LDO/PHF compound, the LDO before and after adsorbed PHF were characterized by XRD, FT-IR, and TG. PHF and LDO/PHF compound are denoted as PHF and LDO-PHF, respectively. In addition, according to the adsorption capacity of PHF, the adsorption products with 175, 348, and 476 mg/g PHF are herein referred to as LDO-PHF175, LDO-PHF348, and LDO-PHF476, respectively. For clarity, the meanings of all the abbreviations are summarized (Table 1).

XRD patterns were obtained using a Bruker D8 ADVANCE X-ray diffractometer (Karlsruhe, German), operating at 40 kV and 40 mA with CuKa radiation. The patterns were recorded over the 2θ range of 3–80° at a scanning speed of 1°/min. FT-IR spectra of KBr pellets in the range

Table 1
Meanings of the abbreviations for the samples.

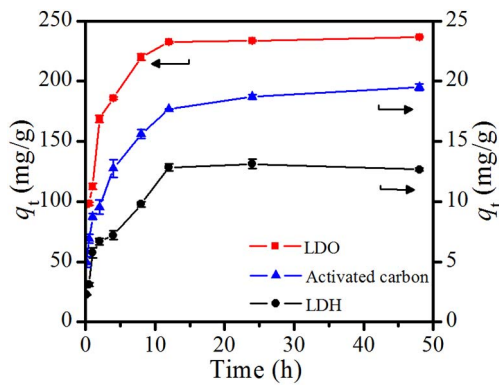| Abbreviation	Meaning
LDH	Layered double hydroxides
LDO	Layered double oxides
PHF	Polyhydroxy fullerenes
LDO-PHF	LDO after PHF adsorption
LDO-PHF175	LDO after 175 mg/g PHF adsorption
LDO-PHF348	LDO after 348 mg/g PHF adsorption
LDO-PHF476	LDO after 476 mg/g PHF adsorption
R-LDH	Rehydrated LDH
LDH/PHF	The mixture of LDH and PHF

Fig. 1. Kinetic of PHF adsorption on LDO, LDH, and activated carbon (the initial concentration of PHF for LDO, LDH, and activated carbon were 250, 25, and 25 mg/L, respectively).

4000–400 cm^{-1} were recorded with a Bruker Vectex 70 spectrometer. TG measurements were carried out on a Netzsch STA 409PC instrument. The samples were heated at a rate of 10 °C/min under a flow of high pure nitrogen (60 mL/min) from 30 to 1000 °C.

3. Results and discussion

3.1. Adsorption results

This work first examined the adsorption kinetics of PHF on the adsorbents, and the results indicated that the equilibration time for PHF adsorption on LDO (on the rehydrated LDH, to be exact), LDH, and activated carbon was approximately 12, 12, and 24 h, respectively (Fig. 1). The adsorption of PHF on the three adsorbents increased sharply within the first 2 h, which could be attributed to the abundant available sites (hydroxyl groups in the layer of LDH) at the initial stage. The relatively slower adsorption on activated carbon may be due to its porous structure, and PHF molecules needed longer time to diffuse into the inner pores. Much higher concentration of PHF was applied for the adsorption on LDO because of its higher adsorption capacity.

The adsorption isotherms of PHF on LDO, LDH, and activated carbon were further obtained in this work (Fig. 2), which showed that the adsorption capacity of PHF on LDO is much higher than that on LDH and activated carbon. The obtained adsorption isotherms for PHF on the three adsorbents were fitted with both Langmuir and Freundlich models (Fig. S1), Two general-purpose equilibrium models were used to fit the experimental data: (i) Langmuir (Eq. (1)) and (ii) Freundlich (Eq. (2)).
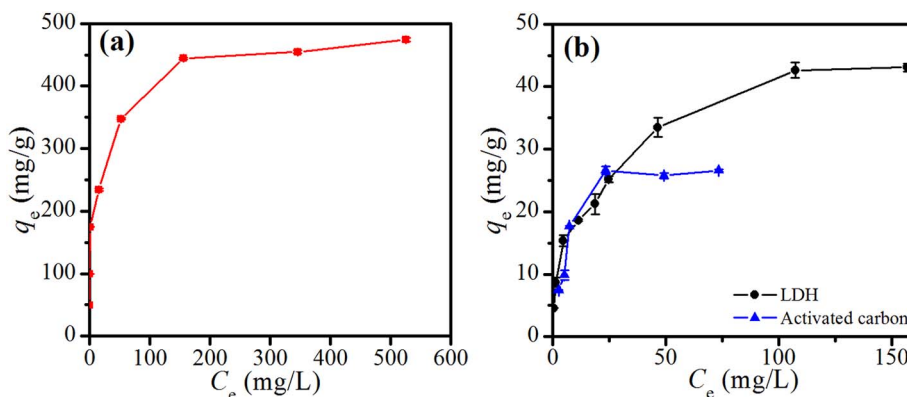
$$q_e = \frac{Q_{max} b C_e}{(1 + b C_e)} \tag{1}$$

Table 2
Parameters of Freundlich and Langmuir isotherms for PHF adsorption on LDO, LDH, and activated carbon.

Adsorbent	Langmuir isotherm			Freundlich isotherm		
	Q_{max} (mg/g)	b (L/mg)	R^2	K_F	n	R^2
LDO	476.19	0.121	0.9981	132.98	4.55	0.8169
LDH	47.40	0.061	0.9777	6.80	2.61	0.9512
Activated carbon	28.49	0.260	0.9827	7.714	2.72	0.6812

$$q_e = k_F C_e^{\ n} \tag{2}$$

where Q_{max} and b are the Langmuir constants related to the loading and energy of adsorption, k_F and n are the Freundlich temperature-dependent constants, C_e is the equilibrium concentration (mg/L), and q_e is the adsorption loading at equilibrium (mg/g), respectively. Compared the Parameters of Freundlich and Langmuir isotherms for PHF adsorption on LDO, LDH, and activated carbon (Table 2), we can found that the Langmuir model fitted these isotherms much better. Furthermore, according to Giles' classification (Giles et al., 1960), the obtained adsorption isotherms for PHF on the three adsorbents belongs to L curve (e.g., the normal or Langmuir isotherms). It suggests monolayer adsorption of PHF molecules on these adsorbents, consistent with the results of other adsorption experiments (Vijayaraghavan et al., 2006; Foo and Hameed, 2010). In addition, the obtained adsorption isotherms for PHF on the three adsorbents also belong to subclass 2 according to Giles' classification (Giles et al., 1960), in which equilibrium data can be represented by Langmuir model and the plateau is represented by the maximum adsorption capacity. Therefore, we can conclude that the maximum adsorption capacity of PHF on LDO is ~476 mg/g, much higher than that on LDH (~47 mg/g) and activated carbon (~28 mg/g) (Table 2). The higher adsorption capacity on LDO indicated that more adsorption sites were available on the surface of LDO, which makes LDO be more efficient adsorbents for PHF.

As is well known, the adsorption capacity of activated carbon strongly depends on its porous structure and large specific surface area, and its micropores play a particular important role for the adsorption of contaminants. However, the size of a single hydrated PHF molecule is ~1.4 nm in combination with the hydration shell (Maciel et al., 2011); in addition, PHF may aggregate with each other to form aggregates with even larger size (20–100 nm) (Djordjevic and Bogdanovic, 2008; Georgieva et al., 2013). The surface area of activated carbon is 1300 m^2/g, with a narrow distribution of micropores at 0.5–1.2 nm. As a result, a large portion of the inner pores, particularly those micropores on activated carbon, may not be accessible by PHF molecules, which is consistent with the adsorption of natural organic matter (Pelekani and Snoeyink, 1999). In addition, with a number of hydroxyl groups (Pelekani and Snoeyink, 1999; Kokubo et al., 2010), PHF molecules may have a weak affinity to the hydrophobic surfaces of

Fig. 2. Equilibrium isotherms for PHF adsorption on (a) LDO (C$_0$ = 50–1000 mg/L), (b) LDH (C$_0$ = 5–200 mg/L), and activated carbon (C$_0$ = 5–100 mg/L).

activated carbon. Therefore, the adsorption efficiency of activated carbon to PHF was the lowest among the three adsorbents. On the other hand, as PHF are negatively charged (Krishna et al., 2010), it may strongly interact with the positively charged LDH surface by electrostatic interaction. Fortner et al. (2012) showed that nC60 nanoparticles (fullerenes aggregates) had higher adsorption capacity on LDH than on montmorillonite and kaolinite. Due to hydroxylation on the surface, nC60 nanoparticles have negative charges, which then enables strong electrostatic interaction between nC60 and the positively charged LDH surface. Similarly, the negatively charged PHF should have strong electrostatic interaction with LDH as well. As such, nC60 and PHF (particularly after forming PHF aggregations) to some extent have similar interaction behaviors with LDH. Fortner et al. (2012) reported a maximum adsorption capacity of 18 mg/g for nC60 on LDH, which is lower than the adsorption of PHF on LDH (~ 47 mg/g). This is reasonable, as PHF are more extensively hydroxylated (i.e., contains more negative charges).

Despite of the strong electrostatic interactions between PHF and LDH, the interlayer spaces of LDH can hardly be used for the adsorption of PHF, because they are not accessible to PHF (as shown by the XRD results and discussed later in this paper). As a result, the adsorption capacity of PHF on LDH was still not significant (Fig. 2b). On the other hand, much higher adsorption capacity of PHF on LDO suggested that more adsorption sites on the rehydrated LDH were occupied by PHF. Previous studies suggested that since the adsorption of anionic contaminants simultaneously happens with the recovering of LDH, the steric hindrance regarding accessing the adsorption sites within the interlayer spaces of LDH can be reduced, leading to an enhanced adsorption of contaminants (Constantino and Pinnavaia, 1995; Zhu et al., 2005).

3.2. Effect of initial pH

The effect of solution pH on the adsorption of PHF on LDH was studied. The adsorption of PHF on LDH was examined at different initial pH values ranging from 4.0–12. The final equilibrium pH values were 8.0–11.8, which may be due to the high pH buffering capacity of LDH. Results showed that the adsorption amounts remain practically constant in the studied pH range and are well in agreement with the literature (Ferreira et al., 2006; Zhu et al., 2005). In addition, LDO has higher pH buffering capacity than LDH during rehydration. Therefore, the adsorption amounts of PHF on LDO and LDH are independent of the pH of bulk solution in pH range of about 4.0–12.

3.3. Effect of co-existing anions on the adsorption of PHF

PHF may co-exist with other inorganic anions in the nature, which may affect its adsorption on LDO. As such, the effect of various co-existing anions such as Cl^-, CO_3^{2-}, SO_4^{2-}, and HPO_4^{2-} (the main existing form of phosphate was HPO_4^{2-} at ~ pH 10) on PHF adsorption on LDO were studied (Fig. 3). Interestingly, Cl^-, CO_3^{2-}, and SO_4^{2-} could slightly enhance the adsorption of the PHF on LDO. The adsorption amount of PHF on LDO decreased drastically in the whole concentration range of PHF with the presence of HPO_4^{2-}. At low concentration of PHF, HPO_4^{2-} showed a significant negative effect on the adsorption of PHF by LDO. With the increase in PHF concentration, the negative effect of HPO_4^{2-} decreased because the competitive effect of PHF was improved.

The effect of co-existing anions on the adsorption process on one hand may affect the surface property of the adsorbents, e.g., occupying some of the adsorption sites (an inhibiting effect) (Das et al., 2006), providing additional adsorption sites (a synergistic effect) (Liu et al., 2015); while, on the other hand, it may affect the properties of the adsorbates, e.g., promoting the aggregation or dispersion of adsorbates (Pavan et al., 1999; dos Reis et al., 2004). As a result, the co-existing ions may have various effects (e.g., promote, inhibit, or no effect) on
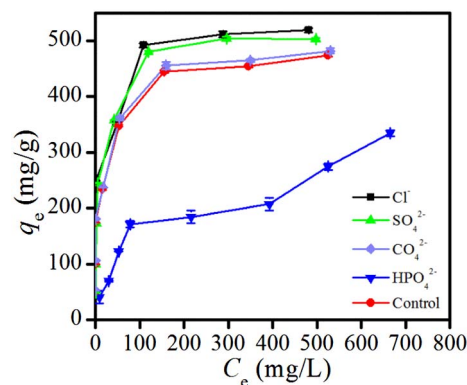

Fig. 3. Equilibrium isotherms for PHF adsorption on LDO with various co-exiting anions.

the adsorption of adsorbates on the adsorbents.

Fortner et al. (2005) indicated that the increase in ionic strength would promote the aggregation of C60, which might have the similar effect on PHF. The addition of NaCl, Na_2CO_3, Na_2SO_4, or NaH_2PO_4 in solution would improve the ionic strength and provide many cations. Therefore, the diffusion double layer of PHF was compressed, leading to a decrease in the repulsive forces between the free PHF and the adsorbed PHF, leading to an enhanced adsorption of PHF on LDO. On the other hand, many researchers found that the competitive effects of Cl^-, CO_3^{2-}, and SO_4^{2-} on the adsorption of anion by LDH was relatively weak and the former was even weaker (Das et al., 2006; Lv et al., 2006). Thus, Cl^-, CO_3^{2-}, and SO_4^{2-} showed a positive effect on the adsorption of PHF by LDO, while Cl^- was more obvious than CO_3^{2-} and SO_4^{2-}. However, phosphate had high affinity towards clays and metal hydroxides, such as LDH, goethite, and ferrihydrite (Geelhoed et al., 1997; Das et al., 2006; Neupane et al., 2014). In addition, Yang et al. (2005) proved that HPO_4^{2-} had stronger interactions with LDH, compared to Cl^-, CO_3^{2-}, and SO_4^{2-}. Therefore, HPO_4^{2-} showed an evident inhibiting effect in the whole concentration range of PHF.

3.4. Characterization results

The XRD patterns of LDO, rehydrated LDH, and LDO-PHF were compared (Fig. 4). The XRD pattern of LDO consisted of only two obvious reflections from MgO, suggesting an almost total decomposition of the original LDH and elimination of most interlayer carbonate anions and water (Das et al., 2006; Laipan et al., 2015). The XRD pattern of rehydrated LDH showed both sharp and symmetrical reflection at 11.6°, indicating the formation of LDH (You et al., 2002). In addition, the XRD pattern of PHF did not show noticeable reflection, suggesting an amorphous structure.

The XRD patterns of PHF adsorbed products indicated that their layered structure was reconstructed. The intensity of these reflections decreased in comparison with rehydrated LDH, demonstrating the less crystallinity of LDO-PHF after calcination and rehydration. The half-peak width values for 003 reflections of LDH, LDO-PHF175, LDO-PHF348, and LDO-PHF476 were 0.609, 0.791, 0.799, and 0.823 nm, respectively, indicating the stacking of c-axis was not uniform. Those results demonstrated that the degree of the stacking order along c-axis for adsorption products was reduced after rehydration because of the presence of PHF. In addition, The XRD patterns of the adsorption products did not show observable shifts in basal spacing, suggesting no significant intercalation into LDH interlayer spaces by PHF. Thus, it could be proposed that only the external surface was available for PHF adsorption, as was also the case for sodium dodecyl sulfate (SDS) adsorption on LDH (Pavan et al., 1999). The probable adsorption models of PHF on LDH and rehydrated LDH were compared (Fig. 5). Rehydrated LDH exposed larger surface and had more adsorption sites for PHF owing to the less uniform stacking order along c-axis in the process
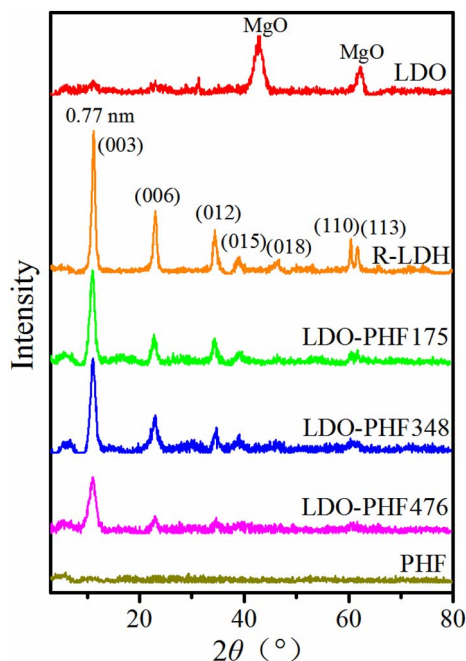
Fig. 4. XRD patterns of LDO, R-LDH, LDO-PHF175, LDO-PHF348, LDO-PHF476, and PHF.

of rehydration.

The TEM image of the adsorption products (LDO-PHF476) is shown in Fig. S2. many nanoparticles with the size of 20–100 nm can be observed, which may be the agglomerate PHF. The uniform distribution of PHF on the surface of LDH may be due to the electrostatic interaction between negatively charged PHF and positively charged LDH.

The FT-IR spectra of rehydrated LDH, PHF, and LDO-PHF were collected (Fig. 6a). For rehydrated LDH, the bands at $3461 \, cm^{-1}$, $1634 \, cm^{-1}$, and $1365 \, cm^{-1}$ were attributed to the H-bonding stretching vibrations of OH^- groups in the brucite-like layers and water molecules, water bending vibration, and the vibrational adsorption of interlayer CO_3^{2-}, respectively (Cavani et al., 1991). With regard to PHF (Fig. 6aV), the spectrum showed a broad O—H band at $3388 \, cm^{-1}$. Three characteristic bands of PHF at 1075, 1376, and $1588 \, cm^{-1}$ can be assigned to νC—O, $\delta_s C$—O—H, and νC=C absorptions, respectively (Xing et al., 2004; Kokubo et al., 2010). A shoulder at $1430 \, cm^{-1}$, is ascribed to the C—C vibration (Hwang and Li, 2010). All of the bands and their possible assignments are listed (Table 3). With increasing adsorption amount of PHF, the blue shift occurred at the bands of 3461 and $1365 \, cm^{-1}$ while the band at $1634 \, cm^{-1}$ appeared red shift for rehydrated LDH. To make clear the variation of the bands, the bans in the range of $2000–1200 \, cm^{-1}$ were fitted (Fig. 6b). With increased adsorption amount of PHF, the relative intensity of the bands at 1376, 1430, and $1588 \, cm^{-1}$ increased, while the relative intensity of the bands at 1365 and $1634 \, cm^{-1}$ decreased. It could be attributed to the

increased amount of adsorbed PHF. Therefore, the characteristic bands of PHF became stronger, while the characteristic bands of LDH became weaker simultaneously. In addition, the relative intensity of the bands at $1365 \, cm^{-1}$ decreased more evidently, indicating the concentration of CO_3^{2-} decreased due to the competition of PHF. Though PHF could not exchange CO_3^{2-} from the interlayer of rehydrated LDH, they might compete with CO_3^{2-} at the external surface of rehydrated LDH, which had more abundant adsorption sites (Fig. 5).

The TG/DTG curve of LDO-PHF476 was compared with those of PHF and rehydrated LDH (Fig. 7). The TG curve of PHF had three stages of mass loss (Fig. 7a). The mass loss stage, occurring from room temperature to 150 °C and 150 °C to 600 °C could be assigned to the loss of bound water and the dehydroxylation of PHF, respectively. Finally, the structural degradation of PHF core started at ~600 °C (Kumar et al., 2014). For rehydrated LDH (Fig. 7b), the first stage of mass loss from room temperature to 264 °C could be attributed to the removal of surface adsorbed and interlayer water molecules. The second mass loss stage (264–700 °C) was from the dehydroxylation of the brucite-like layers and the decomposition of carbonate (Xu et al., 2011).

With regard to LDO-PHF476, three mass loss stages were observed for the TG/DTG curve as well (Fig. 7c). The mass loss of absorbed water molecules occurred from room temperature to 159 °C. The second loss stage, which occurred from 159 °C to 256 °C, might arise from the dehydroxylation of PHF and the loss of interlayer water molecules of LDH. The third stage, with a graduate mass loss from 256 to 1000 °C, could be assigned to the dehydroxylation of the brucite-like layers, the decomposition of carbonate, and the decomposition of PHF core. The pure PHF had a sharp mass loss in the temperature range from 600 to 930 °C, while the mass loss of LDO/PHF476 gradually stabilized above 600 °C.

For comparison purpose, the TG curve of the mixture of LDH and PHF (476 mg PHF with 1.67 g LDH) was determined as well (Fig. 7d). Three mass loss stages on TG curves of LDH/PHF could be attributed to the desorption of water (room temperature to 159 °C), dehydroxylation (159–277 °C), and the decomposition of carbonate (277–600 °C), respectively, which was consistent with the mass loss of LDO-PHF476. However, another mass loss from 600 °C to 1000 °C, which could be assigned to the structural degradation of PHF core. The total mass loss of LDH/PHF was 47.49%, nearly consistent with that of LDO/PHF476 (48.14%). In addition, when the total mass loss reached 45%, the temperature of LDO-PHF476 was 730 °C, higher than that of LDH/PHF (644 °C). This indicated that the thermal stability of PHF was weakened after being adsorbed on LDO, because PHF could disperse more uniformly after adsorption on LDO compared to mechanically mixing with LDH.

4. Conclusion

The adsorption of PHF on LDO, LDH, and activated carbon was investigated. The adsorption capacity of PHF on LDO reached approximately 476 mg/g, much higher than that on LDH (~47 mg/g) and activated carbon (~28 mg/g). All of the three equilibrium adsorption
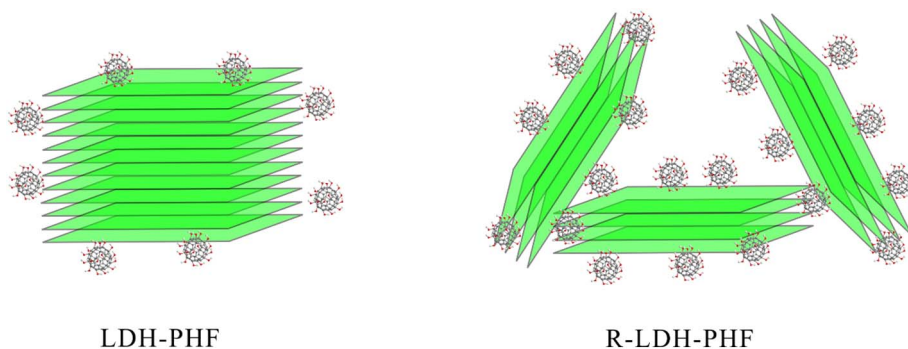
Fig. 5. The probable adsorption models of PHF on LDH and R-LDH.

LDH-PHF
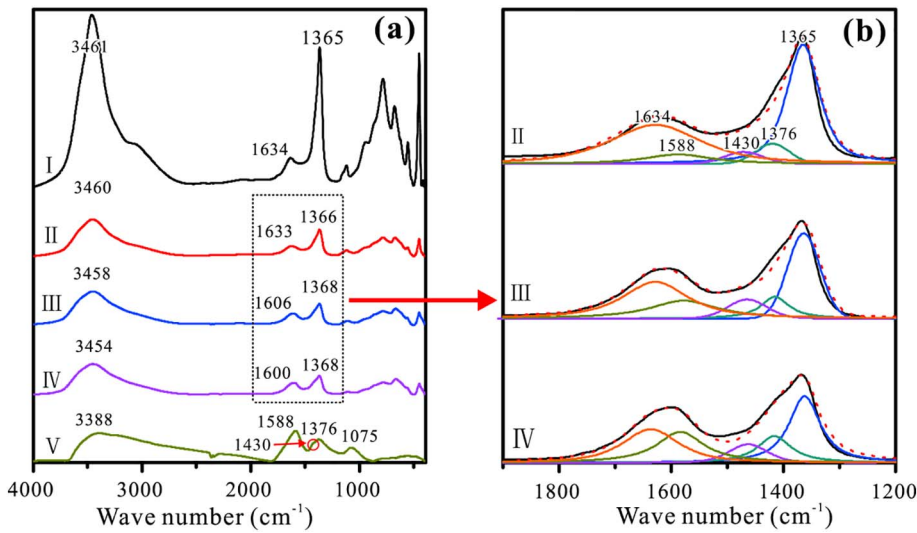
R-LDH-PHF

Table 3

Table summarizing some of the bond types and their range of FT-IR frequencies.

Bond type	Absorption frequency (cm^{-1})
M−OH and H$_2$O stretch	3388–3461
νCO_3^{2-}	≈ 1365
H$_2$O bending	≈ 1634
νC−O	≈ 1075
δ_sC−O−H	≈ 1376
νC=C	≈ 1588
νC−C	≈ 1430

isotherms could be well fitted with the Langmuir equation. The high adsorption capacity of PHF on LDO can be attributed to the enhanced accessibility to the adsorption sites by PHF during structural reconstruction of LDO and the electrostatic interaction between PHF and LDH. Cl$^-$, CO$_3^{2-}$, and SO$_4^{2-}$ could slightly enhance the adsorption of the PHF on LDO, while HPO$_4^{2-}$ showed a profound interfering effect in the whole concentration range of PHF. The XRD, FT-IR, and TG results indicated that the adsorbed PHF could not intercalate into the interlayer spaces of the reconstructed LDH, but could effectively compete with CO$_3^{2-}$ during the adsorption process. Results showed that LDO is a promising material for the treatment of PHF.

Acknowledgment

Appendix A. Supplementary data

Supplementary data to this article can be found online at https://
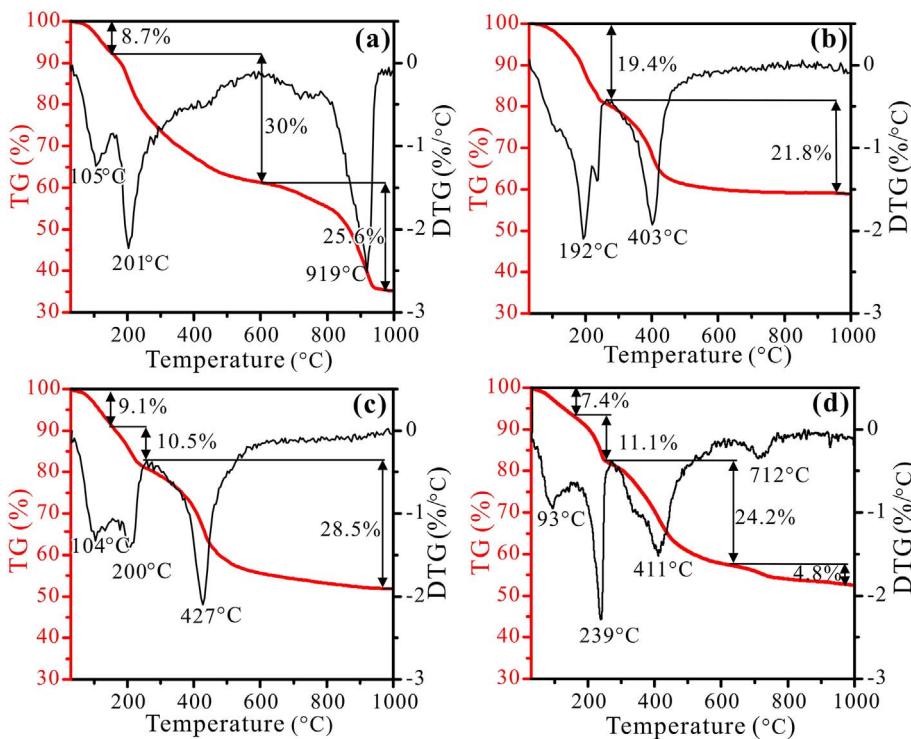

Fig. 7. TG/DTG curves of (a) PHF, (b) R-LDH, (c) LDO-PHF476, and (d) LDH/PHF.

References

Avanasi, R., Jackson, W.A., Sherwin, B., Mudge, J.F., Anderson, T.A., 2014. C60 fullerene soil sorption, biodegradation, and plant uptake. Environ. Sci. Technol. 48, 2792–2797.

Cavani, F., Trifirò, F., Vaccari, A., 1991. Hydrotalcite-type anionic clays: preparation, properties and applications. Catal. Today 11, 173–301.

Cha, C., Su, R.S., Annabi, N., Dokmeci, M.R., Khademhosseini, A., 2013. Carbon-based nanomaterials: multifunctional materials for biomedical engineering. ACS Nano 7, 2891–2897.

Chae, S.R., Hunt, D.E., Ikuma, K., Yang, S., Cho, J., Gunsch, C.K., Liu, J., Wiesner, M.R., 2014. Aging of fullerene C_{60} nanoparticle suspensions in the presence of microbes. Water Res. 65, 282–289.

Chen, Q., Zhu, R., Zhu, Y., Liu, J., Zhu, L., Ma, L., Chen, M., 2016. Adsorption of poly-hydroxy fullerene on polyethylenimine-modified montmorillonite. Appl. Clay Sci. 132-133, 412–418.

Cheng, X., Kan, A.T., Tomson, M.B., 2004. Naphthalene adsorption and desorption from aqueous C60 fullerene. J. Chem. Eng. Data 49, 675–683.

Constantino, V.R., Pinnavaia, T.J., 1995. Basic properties of $Mg_{1\,-\,x}^{2\,+}Al_x^{3\,+}$ layered double hydroxides intercalated by carbonate, hydroxide, chloride, and sulfate anions. Inorg. Chem. 34, 883–892.

Crepaldi, E.L., Tronto, J., Cardoso, L.P., Valim, J.B., 2002. Sorption of terephthalate anions by calcined and uncalcined hydrotalcite-like compounds. Colloids Surf. A Physicochem. Eng. Asp. 211, 103–114.

Dai, L., Chang, D.W., Baek, J.B., Lu, W., 2012. Carbon nanomaterials for advanced energy conversion and storage. Small 8, 1130–1166.

Das, J., Patra, B.S., Baliarsingh, N., Parida, K.M., 2006. Adsorption of phosphate by layered double hydroxides in aqueous solutions. Appl. Clay Sci. 32, 252–260.

Djordjevic, A., Bogdanovic, G., 2008. Fullerenol: a new nanopharmaceutic? Arch. Oncol. 16, 42–45.

Faria, P.C., Orfao, J.J., Pereira, M.F., 2004. Adsorption of anionic and cationic dyes on activated carbons with different surface chemistries. Water Res. 38, 2043–2052.

Ferreira, O.P., de Moraes, S.G., Duran, N., Cornejo, L., Alves, O.L., 2006. Evaluation of boron removal from water by hydrotalcite-like compounds. Chemosphere 62, 80–88.

Foo, K.Y., Hameed, B.H., 2010. Insights into the modeling of adsorption isotherm systems. Chem. Eng. J. 156, 2–10.

Fortner, J., Lyon, D., Sayes, C., Boyd, A., Falkner, J., Hotze, E., Alemany, L., Tao, Y., Guo, W., Ausman, K., 2005. C60 in water: nanocrystal formation and microbial response. Environ. Sci. Technol. 39, 4307–4316.

Fortner, J.D., Solenthaler, C., Hughes, J.B., Puzrin, A.M., Plotze, M., 2012. Interactions of clay minerals and a layered double hydroxide with water stable, nano scale fullerene aggregates (nC60). Appl. Clay Sci. 55, 36–43.

Geelhoed, J.S., Hiemstra, T., Van Riemsdijk, W.H., 1997. Phosphate and sulfate adsorption on goethite: single anion and competitive adsorption. Geochim. Cosmochim. Acta 61, 2389–2396.

Georgieva, A.T., Pappu, V., Krishna, V., Georgiev, P.G., Ghiviriga, I., Indeglia, P., Xu, X., Fan, Z.H., Koopman, B., Pardalos, P.M., Moudgil, B., 2013. Polyhydroxy fullerenes. J. Nanopart. Res. 15.

Gharbi, N., Pressac, M., Hadchouel, M., Szwarc, H., Wilson, S.R., Moussa, F., 2005. [60] fullerene is a powerful antioxidant *in vivo* with no acute or subacute toxicity. Nano Lett. 5, 2578–2585.

Giles, C.H., Macewan, T.H., Nakhwa, S.N., Smith, D.J., 1960. Studies in adsorption part XI: a system of classification of solution adsorption isotherms and its use in diagnosis of adsorption mechanism and measurement of specific surface areas of solid. J. Chem. Soc. 111, 3973–3993.

He, H., Ma, Y., Zhu, J., Yuan, P., Qing, Y., 2010. Organoclays prepared from montmor-illonites with different cation exchange capacity and surfactant configuration. Appl. Clay Sci. 48, 67–72.

Heyman, D., 1991. On the chemical attack of fullerene, soot, graphite, and sulfur with hot perchloric acid. Carbon 29, 684–685.

Hwang, Y.S., Li, Q.L., 2010. Characterizing photochemical transformation of aqueous nC60 under environmentally relevant conditions. Environ. Sci. Technol. 44, 3008–3013.

Isakovic, A., Markovic, Z., Todorovicmarkovic, B., Nikolic, N., Vranjesdjuric, S., Mirkovic, M., Dramicanin, M., Harhaji, L., Raicevic, N., Nikolic, Z., 2006. Distinct cytotoxic mechanisms of pristine versus hydroxylated fullerene. Toxicol. Sci. 91, 173–183.

Jia, G., Wang, H.F., Yan, L., Wang, X., Pei, R.J., Yan, T., Zhao, Y.L., Guo, X.B., 2005. Cytotoxicity of carbon nanomaterials: single-wall nanotube, multi-wall nanotube, and fullerene. Environ. Sci. Technol. 39, 1378–1383.

Jiang, H., Lee, P.S., Li, C., 2012. D carbon based nanostructures for advanced super-capacitors. Energy Environ. Sci. 6, 41–53.

Jordá-Beneyto, M., Suárez-García, F., Lozano-Castelló, D., Cazorla-Amorós, D., Linares-Solano, A., 2007. Hydrogen storage on chemically activated carbons and carbon nanomaterials at high pressures. Carbon 45, 293–303.

Jung, J.-H., Vadahanambi, S., Oh, I.-K., 2010. Electro-active nano-composite actuator based on fullerene-reinforced Nafion. Compos. Sci. Technol. 70, 584–592.

Kokubo, K., Shirakawa, S., Kobayashi, N., Aoshima, H., Oshima, T., 2010. Facile and scalable synthesis of a highly hydroxylated water-soluble fullerenol as a single na-noparticle. Nano Res. 4, 204–215.

Krishna, V., Noguchi, N., Koopman, B., Moudgil, B., 2006. Enhancement of titanium di-oxide photocatalysis by water-soluble fullerenes. J. Colloid Interface Sci. 304, 166–171.

Krishna, V., Singh, A., Sharma, P., Iwakuma, N., Wang, Q., Zhang, Q., Knapik, J., Jiang, H., Grobmyer, S.R., Koopman, B., Moudgil, B., 2010. Polyhydroxy fullerenes for non-invasive cancer imaging and therapy. Small 6, 2236–2241.

Kumar, R., Kumar, P., Naqvi, S., Gupta, N., Saxena, N., Gaur, J., Maurya, J.K., Chand, S., 2014. Stable graphite exfoliation by fullerenol intercalation via aqueous route. New J. Chem. 38, 4922–4930.

Laipan, M., Zhu, R., Chen, Q., Zhu, J., Xi, Y., Ayoko, G.A., He, H., 2015. From spent Mg/Al layered double hydroxide to porous carbon materials. J. Hazard. Mater. 300, 572–580.

Lee, J., Song, W.H., Jang, S.S., Fortner, J.D., Alvarez, P.J.J., Cooper, W.J., Kim, J.H., 2010. Stability of water-stable C60 clusters to OH radical oxidation and hydrated electron reduction. Environ. Sci. Technol. 44, 3786–3792.

Liu, J., Zhu, R., Xu, T., Xu, Y., Ge, F., Xi, Y., Zhu, J., He, H., 2015. Co-adsorption of phosphate and zinc(II) on the surface of ferrihydrite. Chemosphere 144, 1148–1155.

Lv, L., He, J., Wei, M., Evans, D.G., Duan, X., 2006. Uptake of chloride ion from aqueous solution by calcined layered double hydroxides: equilibrium and kinetic studies. Water Res. 40, 735–743.

Lv, L., Wang, Y., Wei, M., Cheng, J., 2008. Bromide ion removal from contaminated water by calcined and uncalcined MgAl-CO3 layered double hydroxides. J. Hazard. Mater. 152, 1130–1137.

Maciel, C., Fileti, E.E., Rivelino, R., 2011. Assessing the solvation mechanism of $C_{60}(OH)_{24}$ in aqueous solution. Chem. Phys. Lett. 507, 244–247.

Markovic, Z., Trajkovic, V., 2008. Biomedical potential of the reactive oxygen species generation and quenching by fullerenes (C60). Biomaterials 29, 3561–3573.

Mauter, M.S., Elimelech, M., 2008. Environmental applications of carbon-based nano-materials. Environ. Sci. Technol. 42, 5843–5859.

Nakagawa, K., Namba, A., Mukai, S.R., Tamon, H., Ariyadejwanich, P., Tanthapanichakoon, W., 2004. Adsorption of phenol and reactive dye from aqueous solution on activated carbons derived from solid wastes. Water Res. 38, 1791–1798.

Neupane, G., Donahoe, R.J., Arai, Y., 2014. Kinetics of competitive adsorption/desorption of arsenate and phosphate at the ferrihydrite–water interface. Chem. Geol. 368, 31–38.

Niu, F., Wu, J., Zhang, L., Li, P., Zhu, J., Wu, Z., Wang, C., Song, W., 2011. Hydroxyl group rich C60 fullerenol: an excellent hydrogen bond catalyst with superb activity, selectivity, and stability. ACS Catal. 1, 1158–1161.

Nowack, B., Bucheli, T.D., 2007. Occurrence, behavior and effects of nanoparticles in the environment. Environ. Pollut. 150, 5–22.

Pavan, P.C., Crepaldi, E.L., Gomes, G.D., Valim, J.B., 1999. Adsorption of sodium dode-cylsulfate on a hydrotalcite-like compound. Effect of temperature, pH and ionic strength. Colloids Surf. A Physicochem. Eng. Asp. 154, 399–410.

Pelekani, C., Snoeyink, V., 1999. Competitive adsorption in natural water: role of acti-vated carbon pore size. Water Res. 33, 1209–1219.

Perez, S., Farre, M., Barcelo, D., 2009. Analysis, behavior and ecotoxicity of carbon-based nanomaterials in the aquatic environment. Trac Trends Anal. Chem. 28, 820–832.

Qu, X., Hwang, Y.S., Alvarez, P.J., Bouchard, D., Li, Q., 2010. UV irradiation and humic acid mediate aggregation of aqueous fullerene (nC60) nanoparticles. Environ. Sci. Technol. 44, 7821–7826.

Reichle, W.T., 1986. Synthesis of anionic clay minerals (mixed metal hydroxides, hy-drotalcite). Solid State Ionics 22, 135–141.

dos Reis, M.J., Silverio, F., Tronto, J., Valim, J.B., 2004. Effects of pH, temperature, and ionic strength on adsorption of sodium dodecylbenzenesulfonate into Mg-Al-CO3 layered double hydroxides. J. Phys. Chem. Solids 65, 487–492.

Sayes, C.M., Fortner, J.D., Guo, W., Lyon, D., Boyd, A.M., Ausman, K.D., Tao, Y.J., Sitharaman, B., Wilson, L.J., Hughes, J.B., 2004. The differential cytotoxicity of water-soluble fullerenes. Nano Lett. 4, 1881–1887.

Song, M., Yuan, S., Yin, J., Wang, X., Meng, Z., Wang, H., Jiang, G., 2012. Size-dependent toxicity of nano-C60 aggregates: more sensitive indication by apoptosis-related Bax translocation in cultured human cells. Environ. Sci. Technol. 46, 3457–3464.

Turco, R.F., Bischoff, M., Tong, Z.H., Nies, L., 2011. Environmental implications of na-nomaterials: are we studying the right thing? Curr. Opin. Biotechnol. 22, 527–532.

Vijayaraghavan, K., Padmesh, T.V., Palanivelu, K., Velan, M., 2006. Biosorption of nickel (II) ions onto *Sargassum wightii*: application of two-parameter and three-parameter isotherm models. J. Hazard. Mater. 133, 304–308.

Wu, J., Alankin, L.B., Li, W., Petrie, L., Welker, C., Fortner, J.D., 2014. Reduction of hydroxylated fullerene (fullerol) in water by zinc: reaction and hemiketal product characterization. Environ. Sci. Technol. 48, 7384–7392.

Xing, G.M., Zhang, J., Zhao, Y.L., Tang, J., Zhang, B., Gao, X.F., Yuan, H., Qu, L., Cao, W.B., Chai, Z.F., Ibrahim, K., Su, R., 2004. Influences of structural properties on stability of fullerenols. J. Phys. Chem. B 108, 11473–11479.

Xu, Z.P., Zhang, J., Adebajo, M.O., Zhang, H., Zhou, C., 2011. Catalytic applications of layered double hydroxides and derivatives. Appl. Clay Sci. 53, 139–150.

Yamawaki, H., Iwai, N., 2006. Cytotoxicity of water-soluble fullerene in vascular en-dothelial cells. Am. J. Physiol. Cell Physiol. 290 (6), C1495–C1502.

Yang, L., Shahrivari, Z., Liu, P.K.T., Sahimi, M., Tsotsis, T.T., 2005. Removal of trace levels of arsenic and selenium from aqueous solutions by calcined and uncalcined layered double hydroxides (LDH). Ind. Eng. Chem. Res. 44, 6804–6815.

Yoon, M., Yang, S., Wang, E., Zhang, Z., 2007. Charged fullerenes as high-capacity hy-drogen storage media. Nano Lett. 7, 2578–2583.

You, Y.W., Zhao, H.T., Vance, G.F., 2002. Adsorption of dicamba (3,6-dichloro-2-methoxy benzoic acid) in aqueous solution by calcined-layered double hydroxide. Appl. Clay Sci. 21, 217–226.

Zhu, M.X., Li, Y.P., Xie, M., Xin, H.Z., 2005. Sorption of an anionic dye by uncalcined and calcined layered double hydroxides: a case study. J. Hazard. Mater. 120, 163–171.

Zhu, R., Molinari, M., Shapley, T.V., Parker, S.C., 2013. Modeling the interaction of na-noparticles with mineral surfaces: adsorbed C60 on pyrophyllite. J. Phys. Chem. A 117, 6602–6611.

Zhu, R., Chen, Q., Zhou, Q., Xi, Y., Zhu, J., He, H., 2016. Adsorbents based on mon-tmorillonite for contaminant removal from water: a review. Appl. Clay Sci. 123, 239–258.